Electronic Supplementary Material (ESI) for Journal of Materials Chemistry A.
This journal is © The Royal Society of Chemistry 2021

SUPPLEMENTAL DATA

A flexible in-plane p-n heterojunction nano-generator with phonon-enhanced photothermoelectric effect to harvest solar energy

Hewu Zhou,[1, 2] Panmeng Tao,[1, 2] Yang Lin, [1, 2] Zihao Chen,[1] Yanjie Zhao,[1, 2] Wei Zeng,[1, 2] Siliang Wang,[1, 2] Zhiliang Chen, [1, 2] Guohua Li,[1, 2] Limin Ruan,[, 1, 2 ,3]*

1 School of Electronics and Information Engineering, Anhui University, No. 111 Jiulong Road, Hefei 230601, Anhui Province, People′s Republic of China

2 National Engineering Research Center for Analysis and Application of Agro-Ecological Big Data, Anhui University, No. 111 Jiulong Road, Hefei 230601, Anhui Province, People′s Republic of China

3. School of Advanced Manufacturing Engineering, Hefei University, No. 99 Jinxiu Road, Hefei, Anhui Province, People′s Republic of China

*Correspondence: ruanlimin@163.com (L. R.)

OUTLINE:

transparent box in the 2nd minute and remove the box in the 16th minute).

Fig. S17. The stability test of as-prepared generator with 3600 secs.

Table S1. The performance parameters of several photothermoelectric materials.

All of the prepared solutions of MWCNT and MXene were deep-dark liquids shown in Fig. S1. To better disperse MWCNT in water, sodium dodecyl benzene sulfonate (SDBS) was applied to the case of surfactant in this study. The MWCNT film was fabricated by Vacuum filtration in order to remove the most of the SDBS in MWCNT film by triple water washing. The treatment processes in detail were presented in Fig. S2, and operated in ambient atmospheres without other protection.

Fig. S1. The digital image of the prepared MWCNT and MXene solution.

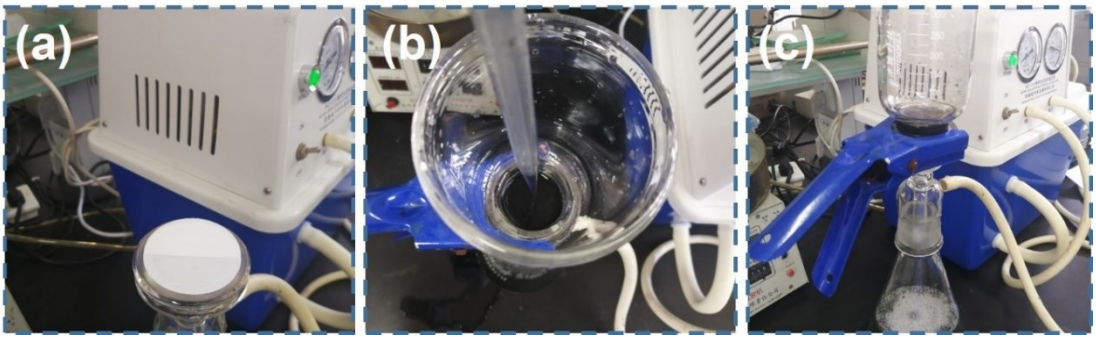

Fig. S2. Vacuum filtration process of the as-fabricated MWCNT film. The digital pictures of (a) first step for placing the filter paper at (b) second steps for transferring the MWCNT solution to the filter bottle and (c) third step for removing the SDBS in MWCNT film.

$Ti_3C_2T_x$ nanosheet was made up from the powder MAX phase by selectively etching Al atom with LiF. MAX powder was purchased from Jilin 11 Technology Co., Ltd, and presents in bulk powder (Fig. S3a). The SEM image of MAX phase (Fig. S3b) showed a layered structural feature.

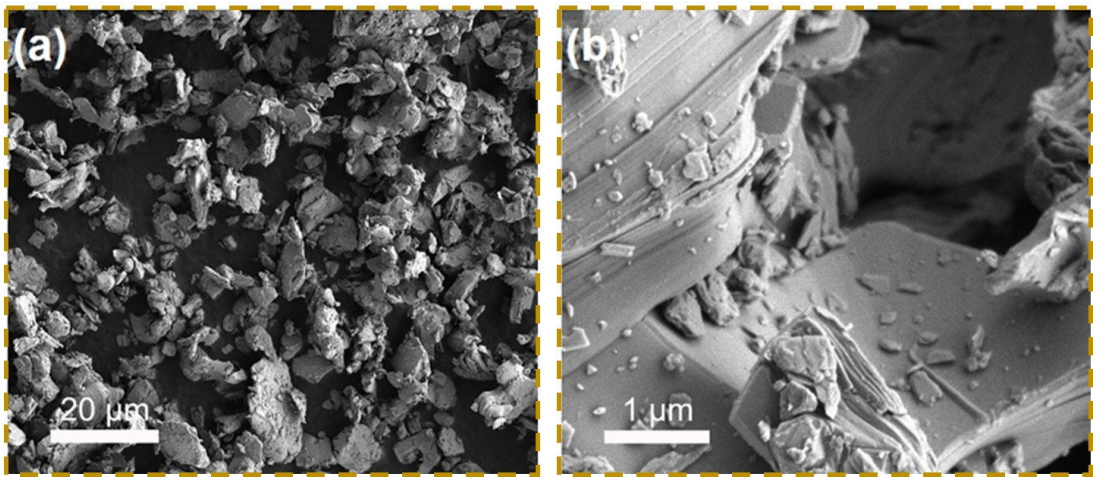

Fig. S3. SEM images of MAX phase at (a) low magnification and (b) high magnification.

The flexibility of CM film was shown in Fig. S4. The thin and light CM film can easy be bended.

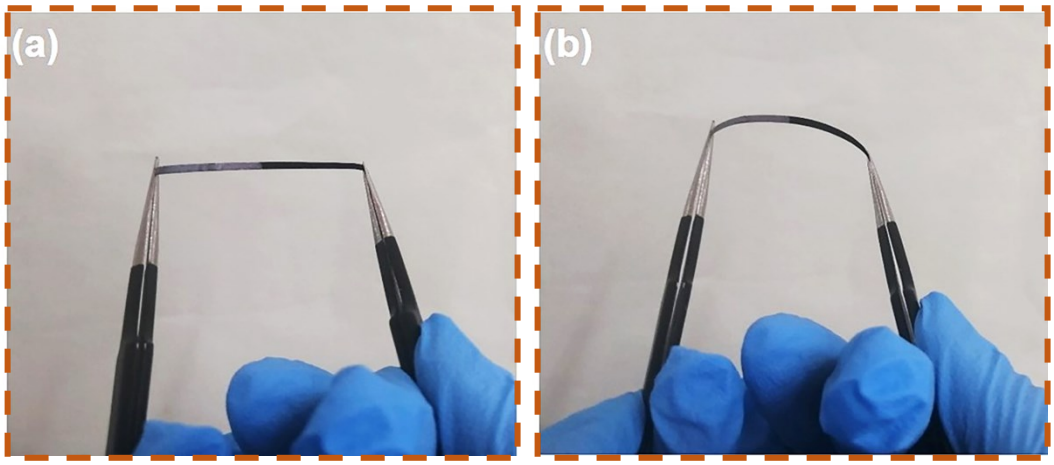

Fig. S4. The flexibility of CM film (a) original status and (b) bent status.

To analysis the inner structure of CM film, the X-ray diffraction (XRD) patterns of MAX phases, MXene side and MWCNT with the filter substrate (Fig. S5) were performed on a Japan Rigaku Smart Lab 9KW X-ray powder diffractometer. Such results kept consistent to previous studies. [1-3]

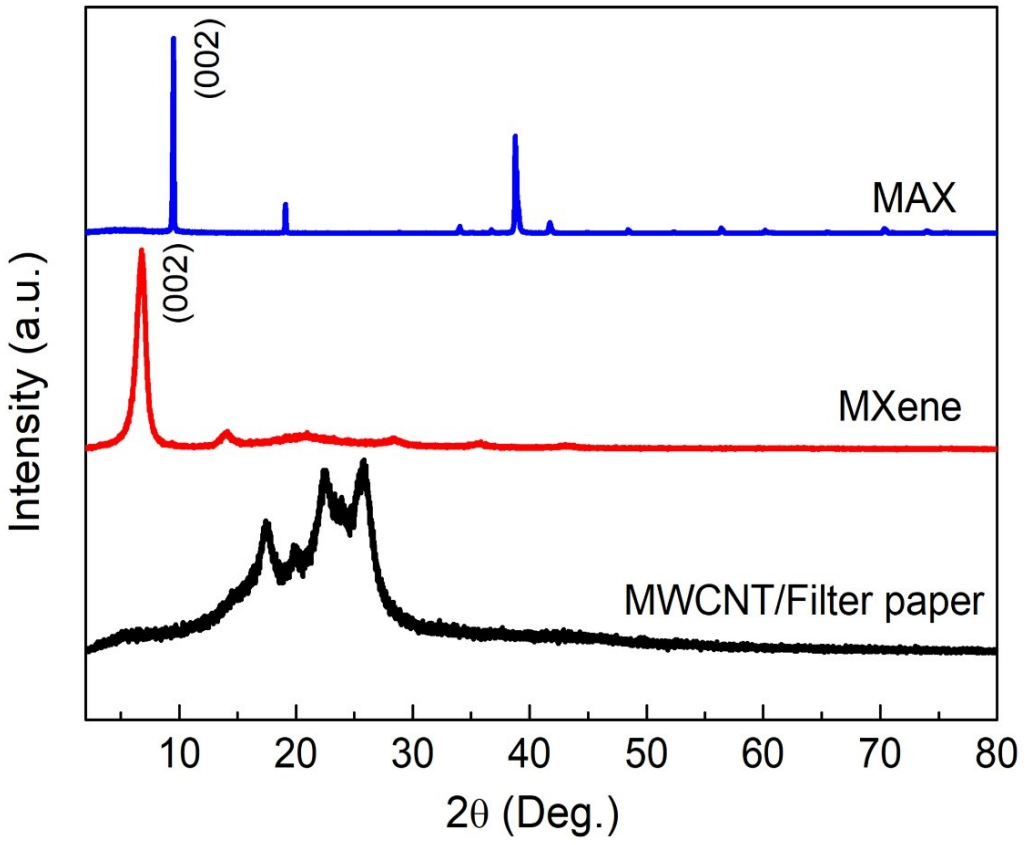

Fig. S5. XRD spectra of MAX phase, MXene and MWCNT with the filter substrate.

The XPS spectra of Ti 2p of MXene side and C 1S of MWCNT side kept good consistent with previous studies [4, 5]. The XPS spectra in Fig. S6a show the contrast curves of the C 1s atomic orbital of MWCNT. According to the fitted curves of the C 1s spectra, the peaks at 284.8 and 285.6 eV represent the C-O band of the MWCNT side. The Carbon 1S binding energy of MXene side at 282.2 eV was observed, which is the most intense peak corresponding to C-Ti-T_x. The peaks at 282.6, 284.7, and 285.5 eV were identified to C-C, C-H and C–O (Fig. S6b). The Ti 2p spectra reveals the presence of Ti(II) and Ti(III) bonds at 455.9 and 458.8 eV, respectively (Fig. S6c).

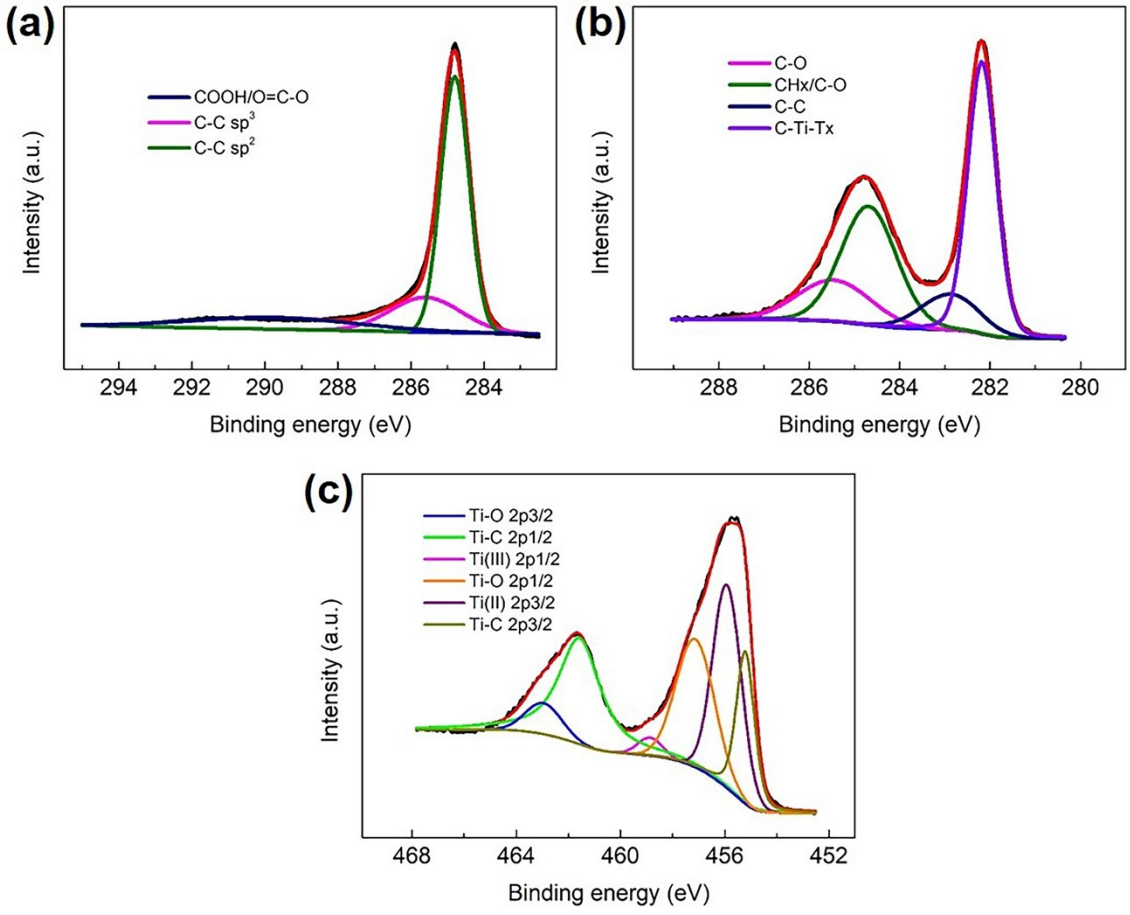

Fig. S6. XPS spectra of MWCNT and MXene with (a) high-resolution C 1s spectra of MWCNT, (b) high-resolution C 1s spectra of MXene and (c) high-resolution Ti 2p spectra of MWCNT.

A home-made Seebeck measuring device was designed by Pelties cooler, thermocouple and other electrical test equipment. The scheme was shown in Fig. S7. The data of temperature and voltage were recorded by a KEYSIGHT 34470A nanovoltmeter. The photo of laser test was shown in Fig. S8. Two probe stations with gold coated copper probe were applied to output electrical signals whet the laser irradiated the interface between MWCNT and MXene side.

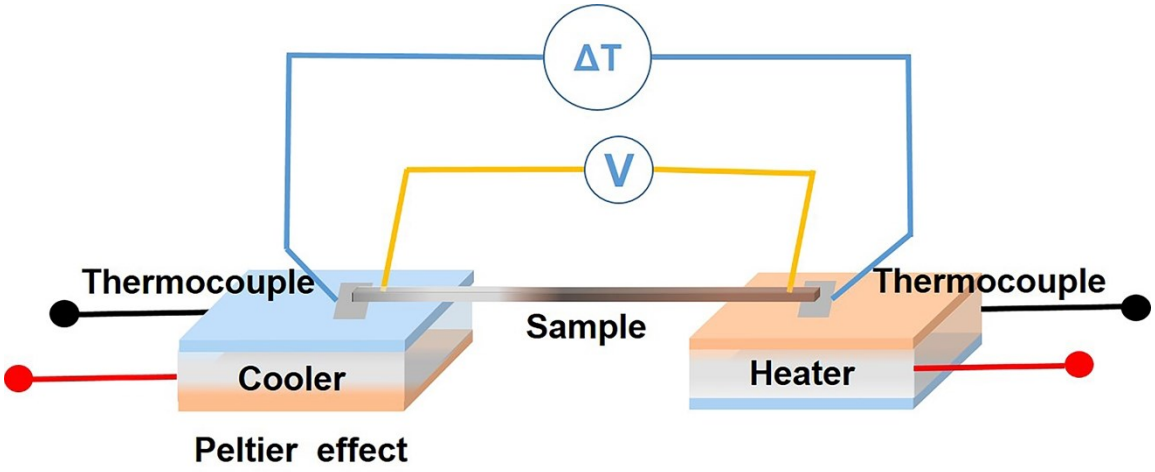

Fig. S7. Home-made Seebeck measuring device using Pertier effect.

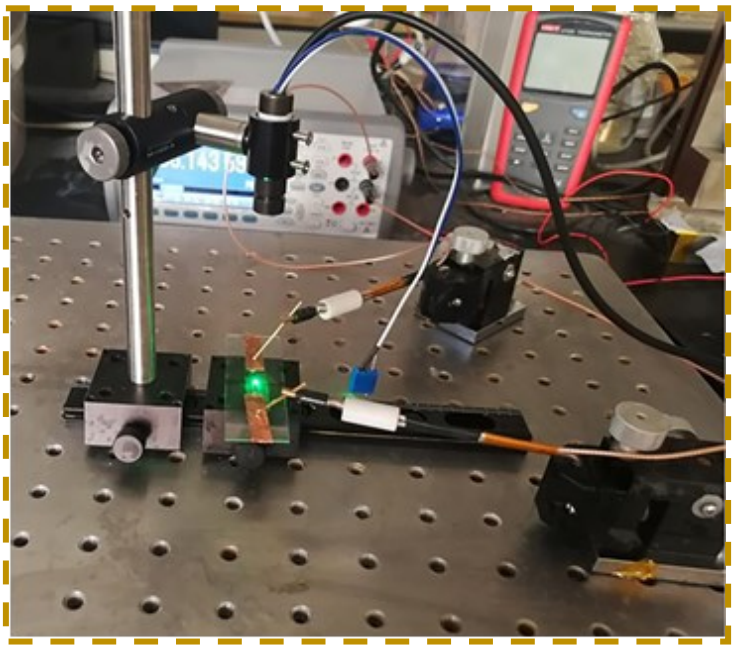

Fig. S8. The digital image of laser test process.

The output voltages of CM film were measured when the interface was illuminated at different laser power (Fig. S9). It can be concluded from Fig. S9f that the output voltages were presented in the direct proportional function of the laser power.

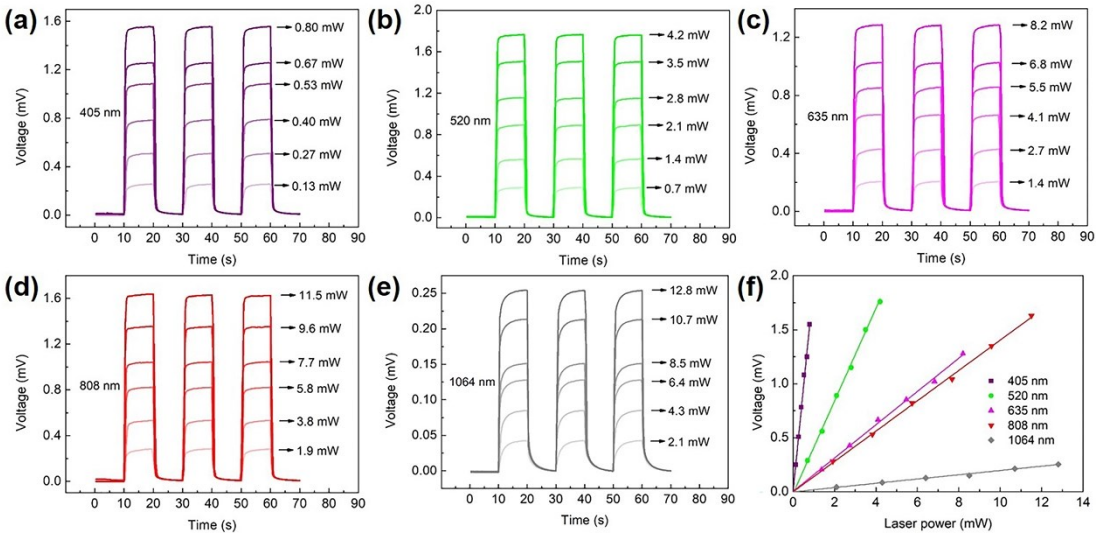

Fig. S9. The output voltages of CM film under the irradiation of (a) 405 nm, (b) 520 nm, (c) 635 nm, (d) 808 nm and (e)1064 nm with different laser power. (f) The relationship between the output voltage of CM film and laser power.

The CM film was sealed with two 20 × 3 × 2 mm PDMS slices, and the output voltage under AM 1.5G simulated sunlight was measured (Fig. S10). The results showed that the output voltage of the CM film with PDMS reached 184 μV after 10 min, which was about 39 μV lower than that of the CM film with transparent box and more jitter. In order to further explore, UV-Vis test was performed on PDMS, and it was found that PDMS had obvious absorption with ultraviolet and infrared light, indicating that PDMS blocked a certain amount of light and heat.

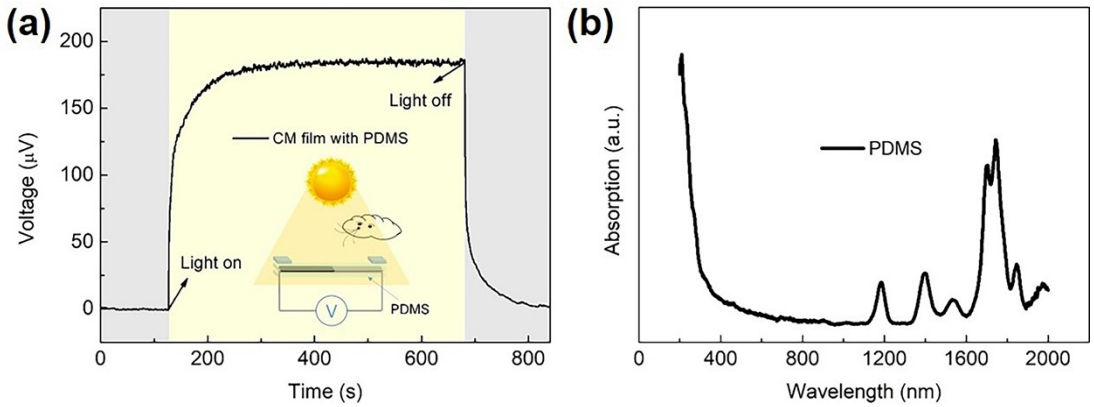

Fig. S10. (a) The output voltage under AM 1.5G simulated sunlight irradiation, (b) The UV-Vis absorption spectrum of CM film covered by PDMS

Fig. S11a is a model diagram of CM film with vertical structure. The MWCNT terminal is positive and the MXENE terminal is negative. The output voltage of vertical-structured CM film under AM 1.5G simulated sunlight was shown in Fig. S11b, which reaches 34 μV.

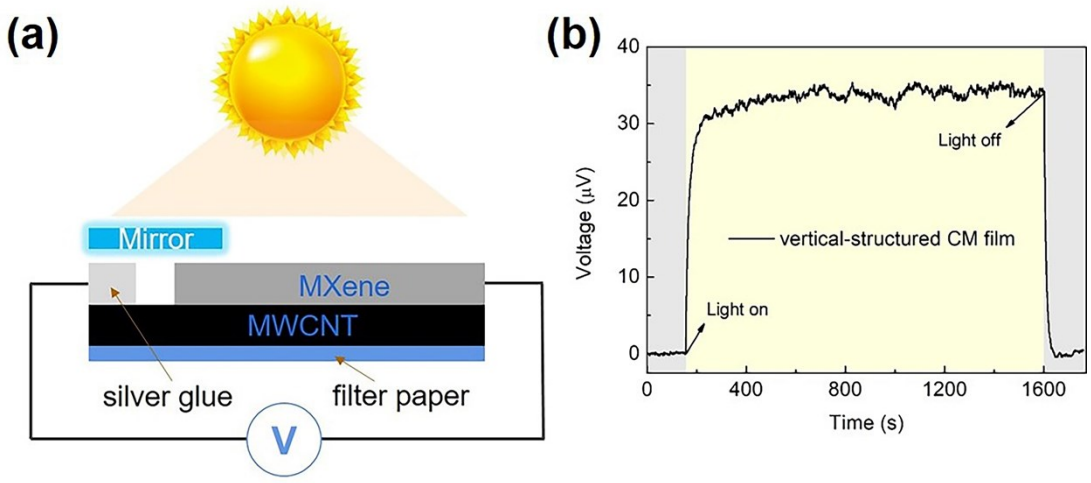

Fig. S11. (a) Model diagram of CM film with vertical structure. (b) The output voltage of vertical-structured CM film under AM 1.5G simulated sunlight

The output voltage of CM film under infrared lamp was recorded and showed in Fig. S12. It was seen that the fluctuation of output voltage was evident and also showed a slow decline during the test. Such result indicated that CM film was sensitive to the temperature, and proved to the action of the PTE effect for the voltage response output.

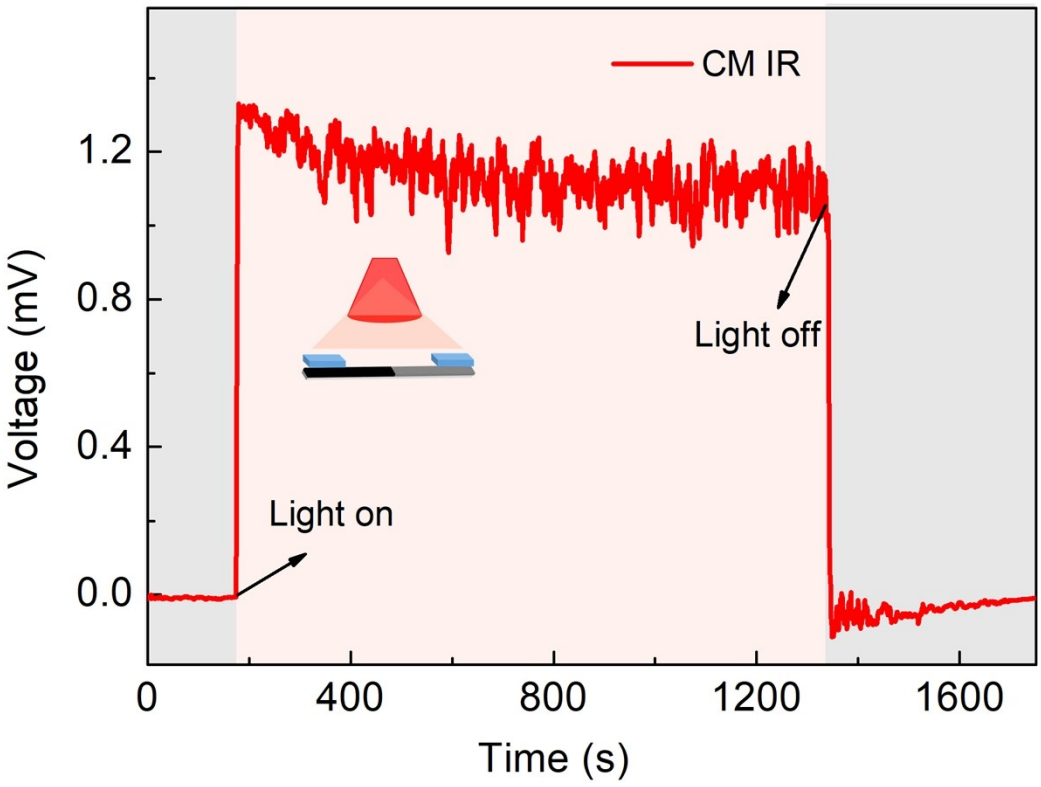

Fig. S12. The output voltage of CM film under infrared lamp

To analysis the ambient temperature during the test process, the ambient temperatures with transparent box and without transparent box were recorded shown in Fig. S13. Through out of the whole test, the temperature without the transparent box showed slow increasement. While, the temperature increased when the CM film covered with a transparent box, and get the maximum value of 314 K.

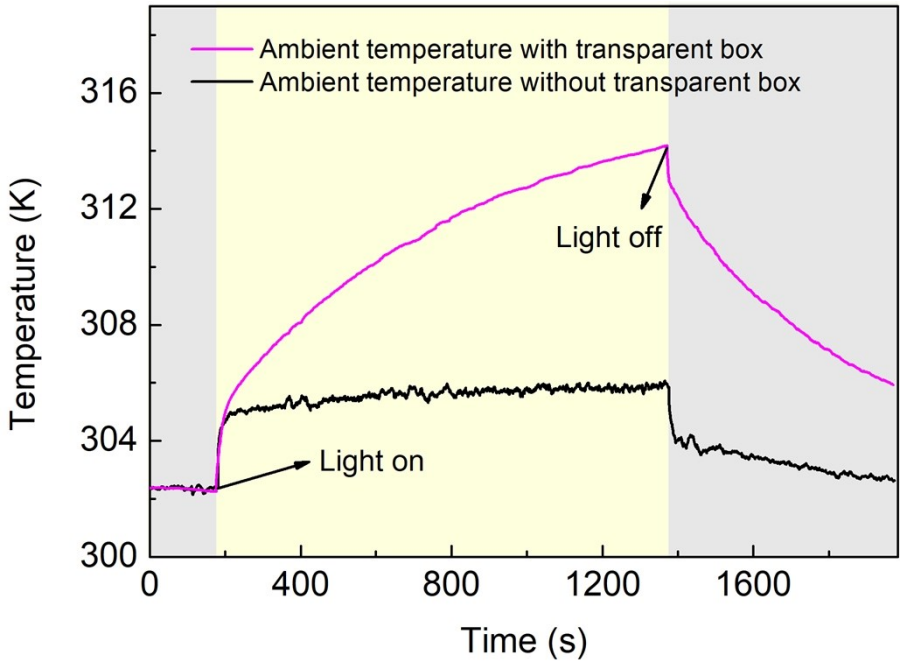

Fig. S13. The ambient temperatures with transparent box and without transparent box.

The output voltage of CM film after bending for 500 times could still maintain 90% of original value (Fig. S14). However, the output voltage of CM film decreased when bending times exceeded 500 times.

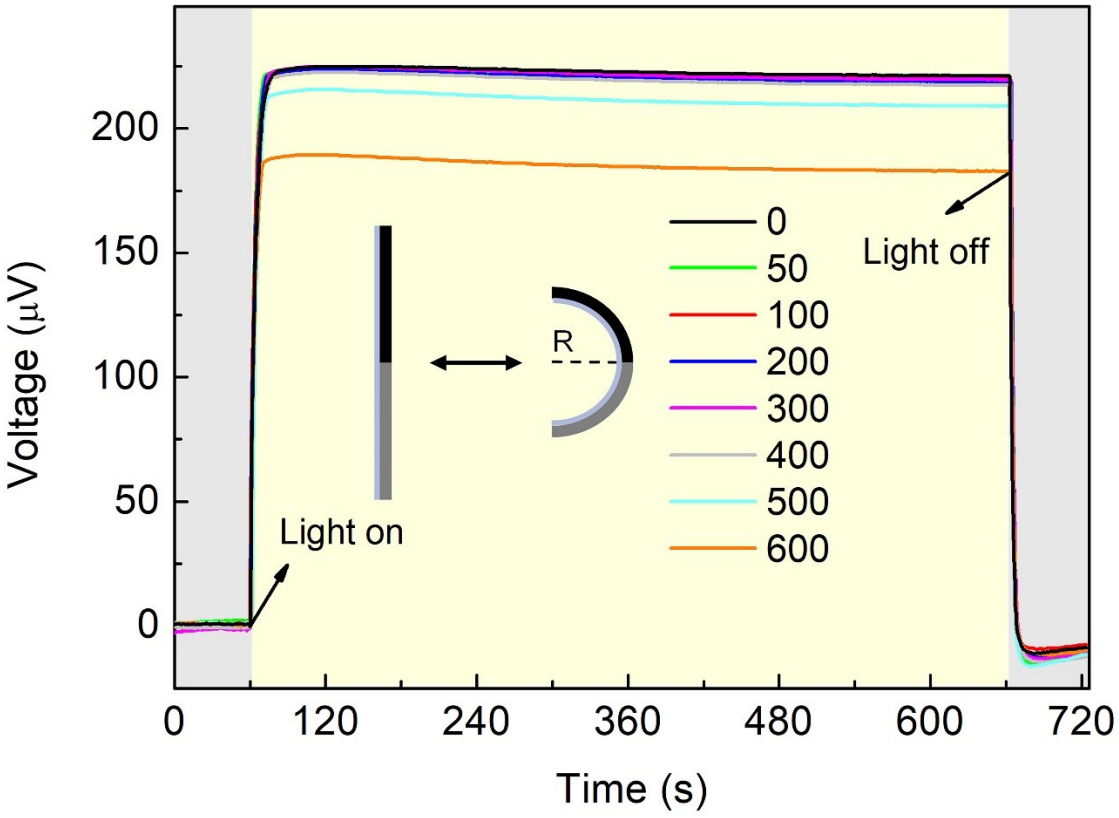

Fig. S14. Output voltages of CM film after bending for different times under the irradiation of AM 1.5G simulated sunlight (with a radius of curvature of 6.4 mm).

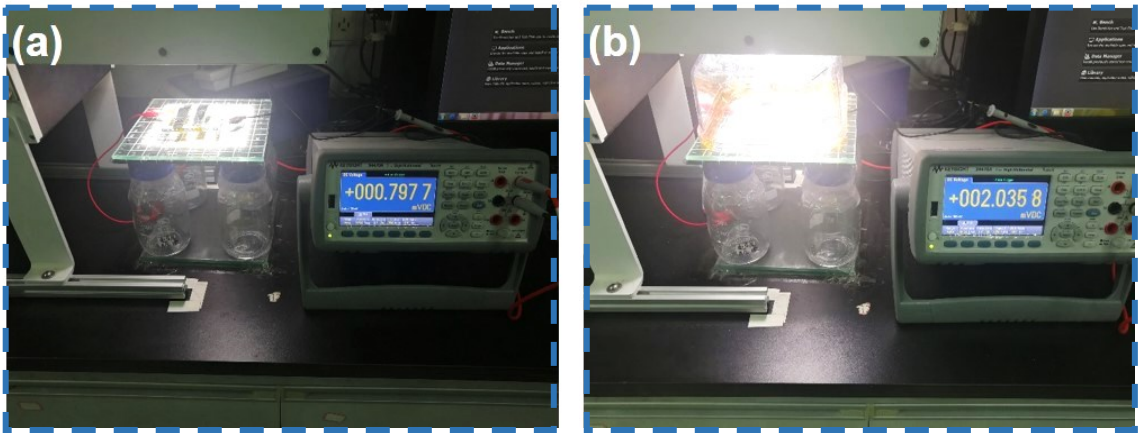

Fig. S15. Photo-induced voltage measurement of the nano-generator under the irradiation of AM 1.5G simulated sunlight (a) without transparent box and (b) with transparent box.

The ambient temperature under a simulated sunlight was recorded shown in Fig. S16. When the CM film covered with a transparent box, the temperature of CM film increased steadily, and reached to the maximum value of 313.2 K, which was similar to that of the single CM film test.

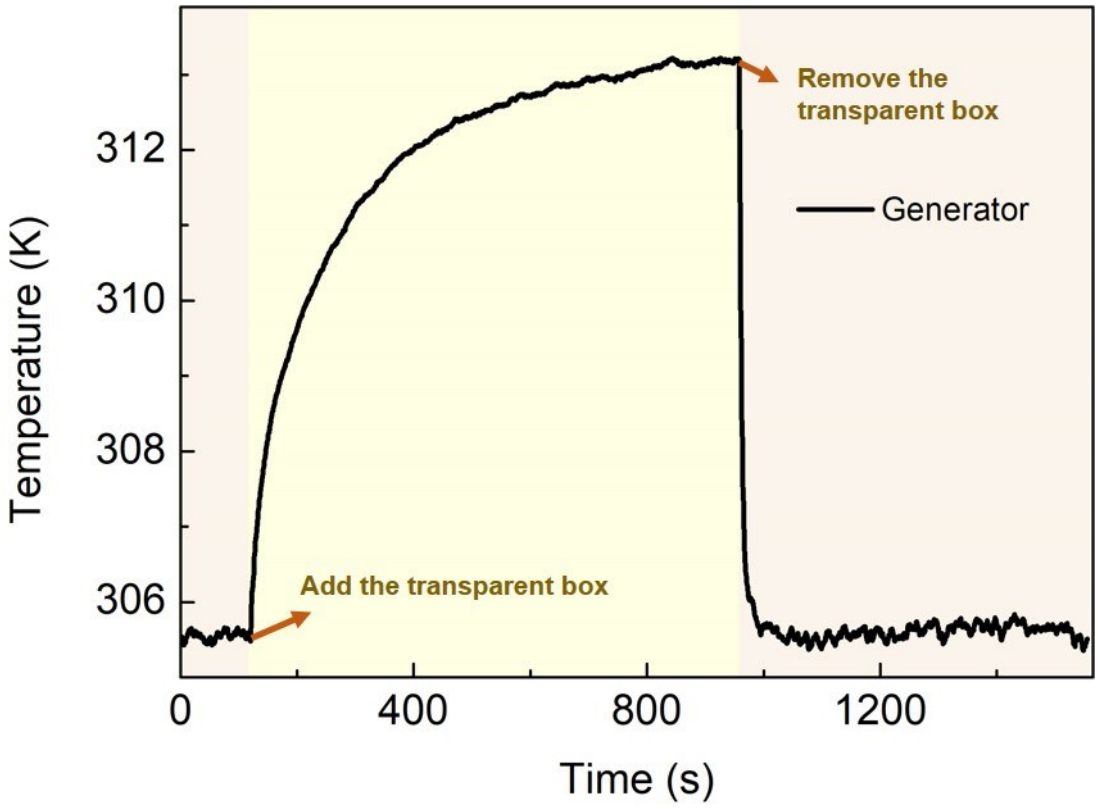

Fig. S16. The ambient temperature under the irradiation of AM 1.5G simulated sunlight (cover the transparent box in the 2nd minute and remove the box in the 16th minute).

The output voltage of the generator with transparent box was measured under AM 1.5G simulated sunlight irradiation for one hour (Fig. S17), which can reach 2 mV. The results showed the reliable stability of the generator.

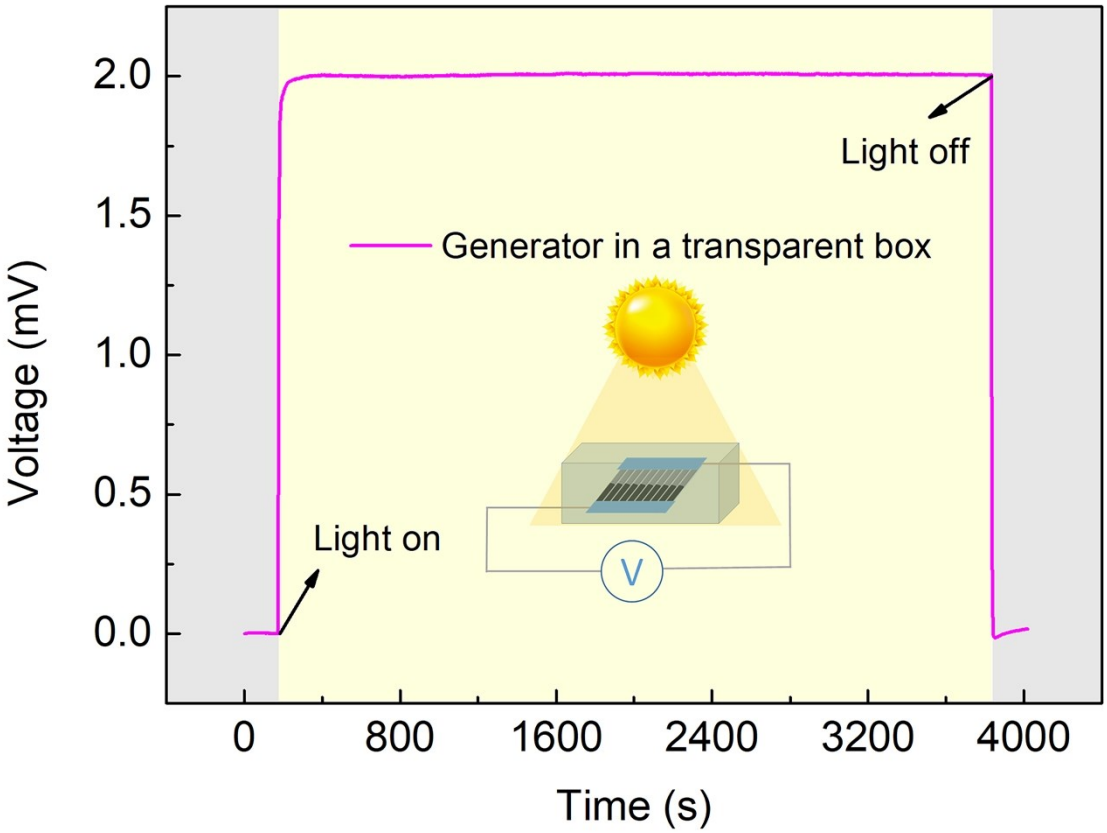

Fig. S17. The stability test of as-prepared generator with 3600 secs.

Table S1 lists the performance parameters of several photothermoelectric materials at room temperature. [6-10] The carrier conductivities of MWCNT and MXene side are 5.71 and 640 $S \cdot cm^{-1}$. Consequently, the PF (Power Factor) of MWCNT and MXene are 0.05 and 1.6 $\mu W \cdot m^{-1} \cdot K^{-2}$, which can better meet the requirements for PTE devices.

Table S1 The performance parameters of several photothermoelectric materials.

Sample	σ [S·cm−1]	*S* [μV·K−1]	PF [μW·m−1·K−2]	Reference
TEG-N2200	0.17	-153	0.4	6
p(gNDI-gT2)	0.3	-93	0.4	7
BBL	1.2	-60	0.43	9
ClBDPPV	0.62	-99	0.63	8
2DQQT-S	0.008	-655	0.34	10
2DQQT-Se	0.29	-217	1.4	10
MXene	640	-5.03	1.6	this work
MWCNT	5.71	10.02	0.05	this work

References

1 A. Sengupta, B.V.B. Rao, N. Sharma, S. Parmar, V. Chavan, S.K. Singh, S. Kale and S. Ogale, Nanoscale, 2020, 12, 8466-8476.

2 K. Rasool, M. Helal, A. Ali, C.E. Ren, Y. Gogotsi and K.A. Mahmoud, ACS Nano, 2016, 10, 3674-3684.

3 B. Wang, A. Zhou, F. Liu, J. Cao, L. Wang and Q. Hu, J. Adv. Ceram., 2018, 7, 237-245.

4 M.A.S.M. Haniff, S.M. Hafiz, K.A. Wahid, Z. Endut, M.I. Syono, N.M. Huang, S.A. Rahman and I.A. Azid, J. Mater. Sci., 2017, 52, 6280-6290.

5 Q. Xue, Z. Pei, Y. Huang, M. Zhu, Z. Tang, H. Li, Y. Huang, N. Li, H. Zhang and C. Zhi, J. Mater. Chem. A, 2017, 5, 20818-20823.

6 J. Liu, L. Qiu, R. Alessandri, X. Qiu, G. Portale, J. Dong, W. Talsma, G. Ye, A.A. Sengrian, P.C.T. Souza, M.A. Loi, R.C. Chiechi, S.J. Marrink, J.C. Hummelen and L.J.A. Koster, Adv. Mater., 30, 1704630.

7 D. Kiefer, A. Giovannitti, H. Sun, T. Biskup, A. Hofmann, M. Koopmans, C. Cendra, S. Weber, L.J. Anton Koster, E. Olsson, J. Rivnay, S. Fabiano, I. McCulloch and C. Muller, ACS Energy Lett., 2018, 3, 278-285.

8 X. Zhao, D. Madan, Y. Cheng, J. Zhou, H. Li, S.M. Thon, A.E. Bragg, M.E. DeCoster, P.E. Hopkins and H.E. Katz, Adv. Mater., 2017, 29, 1606928.

9 S. Wang, H. Sun, U. Ail, M. Vagin, P.O. Persson, J.W. Andreasen, W. Thiel, M. Berggren, X. Crispin, D. Fazzi and S. Fabiano, Adv. Mater., 2016, 28, 10764-10771.

10 D. Yuan, Y. Guo, Y. Zeng, Q. Fan, J. Wang, Y. Yi and X. Zhu, Angew. Chem. Int. Ed. Engl., 2019, 58, 4958-4962.